

Footprints of the Kitaev spin liquid in the Fano lineshapes of the Raman active optical phonons

Kexin Feng,¹ Swetlana Swarup,¹ and Natalia B. Perkins¹

¹*School of Physics and Astronomy, University of Minnesota, Minneapolis, MN 55455, USA*

(Dated: August 23, 2021)

We develop a theoretical description of the Raman spectroscopy in the spin-phonon coupled Kitaev system and show that it can provide intriguing observable signatures of fractionalized excitations characteristic of the underlying spin liquid phase. In particular, we obtain the explicit form of the phonon modes and construct the coupling Hamiltonians based on D_{3d} symmetry. We then systematically compute the Raman intensity and show that the spin-phonon coupling renormalizes phonon propagators and generates the salient Fano lineshape. We find that the temperature evolution of the Fano lineshape displays two crossovers, and the low temperature crossover shows pronounced magnetic field dependence. We thus identify the observable effect of the Majorana fermions and the Z_2 gauge fluxes encoded in the Fano lineshape. Our results explain several phonon Raman scattering experiments in the candidate material α -RuCl₃.

Introduction.— Raman spectroscopy has proven to be a sensitive experimental probe to study the ground state properties and the dynamics of various strongly correlated systems [1]. For magnetic insulators, Raman process couples to the dynamically induced electron-hole pair, that connects to the low-energy magnetic states. In magnetically ordered states, the magnetic Raman response shows polarization-dependent peak structure, arising predominantly from one- and two-magnon excitations [2–7]. In quantum spin liquid (QSL) phase, the Raman spectrum of such low-energy states reveals characteristic low-energy continua, which are fundamentally different from the dispersive collective modes in ordered states. These continua reflect the fractionalization of spins, a hallmark of QSL [8–16].

Recently, significant efforts have been made in the investigation of quantum spin-liquid (QSL) state of matter. Mott insulators with strong spin-orbit coupling, e.g α -RuCl₃ [17–28], are promising to realize Kitaev QSL. This QSL is motivated by the famous Kitaev spin model with bond-dependent Ising interactions on a two-dimensional honeycomb lattice [29]. It is exactly solvable with known gapless QSL ground state. In this model, the spins fractionalize into static Z_2 gauge fluxes and itinerant Majorana fermions amenable to experimental detection.

While various dynamical probes [9, 14, 30–34] have been exploited in several materials to look for signatures of spin fractionalization and their proximity to the Kitaev QSL, employing phonon dynamics and the spin-lattice coupling to detect Kitaev QSL is less investigated. It was recently suggested that sound attenuation from the phonon decaying into a pair of Majorana fermions [35–37] and the Hall viscosity induced by time-reversal breaking spin Hamiltonian [36, 37] may potentially serve as such probe. The importance of the spin-phonon coupling in the Kitaev materials is also shown in the interpretation of the thermal Hall transport measurements [38–40].

In this letter, we focus on the Raman spectroscopy of optical phonons, and particularly the salient Fano line

shape, which arises when the phonon resonance peak couples to the magnetic continuum [41]. This effect is attributed to *spin-dependent* electron polarizability [42, 43], which involves a microscopic description of both spin-photon coupling and spin-phonon couplings. A recent work Ref. [16] shows that even the simplest form of the couplings can give rise to the Fano line shape. In the experimental studies of the candidate material α -RuCl₃ [23–27, 44], the pronounced temperature and field dependence of Fano lineshape indicate rich information about the underlying spin liquid phase that awaits exploration. However, up to now a clear theoretical description of the Raman scattering in a Kitaev spin-phonon coupled system is still missing, mainly due to the lack of proper description of spin-phonon and spin-photon couplings [16].

Here, we make use of the D_{3d} group symmetry of the Kitaev model [45] and propose a theory to describe the Raman scattering of the Kitaev spin-phonon coupled system. We show that our theory, in which the spin-phonon coupling and spin-photon coupling are explicitly built from the symmetry constraints, quantitatively characterizes the temperature evolution and field dependence of the Fano lineshape of two low-energy optical phonons, observed in the Raman scattering experiments in α -RuCl₃ [23–27, 44]. These results reveal clear effects of the Majorana fermions and the Z_2 fluxes, which provide observable signatures for experimental detection of Kitaev QSL.

Model.— We consider the spin-phonon Hamiltonian

$$H = H_s + H_{\text{ph}} + H_{\text{s-ph}}. \quad (1)$$

The *first* term is the extended Kitaev honeycomb model [29], $H_s = -J \sum_{\alpha, \mathbf{r} \in A} \sigma_{\mathbf{r}}^{\alpha} \sigma_{\mathbf{r} + \mathbf{M}_{\alpha}}^{\alpha} - \kappa \sum_{\langle \mathbf{r}, \mathbf{r}', \mathbf{r}'' \rangle_{\alpha\gamma}} \sigma_{\mathbf{r}}^{\alpha} \sigma_{\mathbf{r}'}^{\beta} \sigma_{\mathbf{r}''}^{\gamma}$, where $\sigma_{\mathbf{r}}^{\alpha}$ are the Pauli matrices, $\alpha = x, y, z$ and \mathbf{M}_{α} are nearest neighbor vectors; J denotes the Kitaev interaction; κ is the strength of the time reversal symmetry breaking term, which mimics the effect of an external magnetic field [29]. The three-spin link

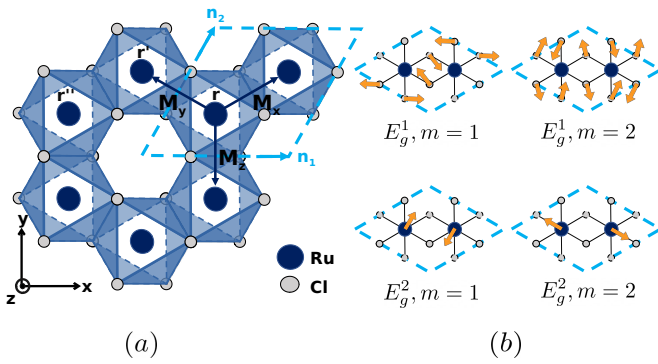


FIG. 1. (a) Crystal structure of α -RuCl₃. The unit cell shown in blue dashed lines is defined by $\mathbf{n}_1 = (\sqrt{3}, 0)$ and $\mathbf{n}_2 = (\frac{3}{2}, \frac{\sqrt{3}}{2})$ and includes two Ru³⁺ and six Cl⁻ ions. $\mathbf{M}_{x,y} = (\pm \frac{\sqrt{3}}{2}, \frac{1}{2})$ and $\mathbf{M}_z = (0, -1)$ are nearest neighbor vectors. The sites $\mathbf{r}, \mathbf{r}', \mathbf{r}''$ form a generic three-spin link $\langle \mathbf{r}, \mathbf{r}', \mathbf{r}'' \rangle_{yx}$ as described in the text. (b) Visualization of the eigenmodes of E_g^1 and E_g^2 phonons in xy plane, obtained by linear representation theory (See supplementary material).

notation $\langle \mathbf{r}, \mathbf{r}', \mathbf{r}'' \rangle_{\alpha\gamma}$ labels bonds $\mathbf{r}\mathbf{r}'$, $\mathbf{r}'\mathbf{r}''$ by type α, γ respectively and $\beta \neq \alpha, \gamma$. $\mathbf{r}, \mathbf{r}', \mathbf{r}''$ are counter-clockwise ordered adjacent sites (see Fig. 1 (a)). This Hamiltonian has a symmetry described by D_{3d} point group [46].

H_s is exactly solvable by the four Majorana fermion representation of spin [29], $\sigma_{\mathbf{r}}^{\alpha} = i b_{\mathbf{r}}^{\alpha} c_{\mathbf{r}}$. In this representation, $H_s = \frac{1}{4} \sum_{\langle \mathbf{r}\mathbf{r}' \rangle} h_{\mathbf{r}\mathbf{r}'} c_{\mathbf{r}} c_{\mathbf{r}'}$, where $h_{\mathbf{r}\mathbf{r}'} = 2J i \eta_{\mathbf{r}\mathbf{r}'} + 2\kappa i \eta_{\mathbf{r}\mathbf{r}'} \eta_{\mathbf{r}'\mathbf{r}''}$ is the Hamiltonian matrix and $\eta_{\mathbf{r}\mathbf{r}'} = i b_{\mathbf{r}}^{\alpha} b_{\mathbf{r}'}^{\alpha} = \pm 1$ is the static Z_2 gauge field on the α -bond, which generates conserved Z_2 fluxes. Within each flux sector, H_s can be further diagonalized to be $H_s = \sum_i \epsilon_i (\beta_i^{\dagger} \beta_i - 1/2)$, where ϵ_i are the fermionic energy levels and $\beta_i^{\dagger}, \beta_i$ correspond to the fermionic eigenmodes. Hereafter [47], the energy and temperature unit will be J unless specified, which is estimated to be $J \approx 2\text{meV} = 23K$ according to Ref. [23].

The *second* term in Eq.(1) is the free phonon Hamiltonian $H_{\text{ph}} = H_{\text{ph}}(p_i(\mathbf{r}), q_i(\mathbf{r}))$, where $q_i(\mathbf{r}) = (x_1, y_1, z_1, \dots, x_8, y_8, z_8)_{\mathbf{r}}$ denotes the displacement field in a unit cell at \mathbf{r} , which contains two Ru³⁺ and six Cl⁻ ions (see Fig.1 (a) and Fig.4 in the supplementary material (SM)). $p_i(\mathbf{r})$ is the corresponding momentum. Hereafter, we will drop the \mathbf{r} dependence in phonon fields, since the long wavelength of incident light leads to uniform lattice vibrations. As shown in the SM, using the D_{3d} symmetry constraint $[D_{3d}, H_{\text{ph}}] = 0$, the eigenmodes of H_{ph} are solved to be the irreducible representations (irreps) of the symmetry group, which are written as linear superposition of the displacement field. In this work, we focus on the two low-energy phonon modes in the Raman spectroscopy [23, 24, 27]: E_g^1 and E_g^2 , whose energies (around 14 meV and 20 meV respectively) are comparable to the magnetic continuum. These modes are both two-fold degenerate and are explicitly

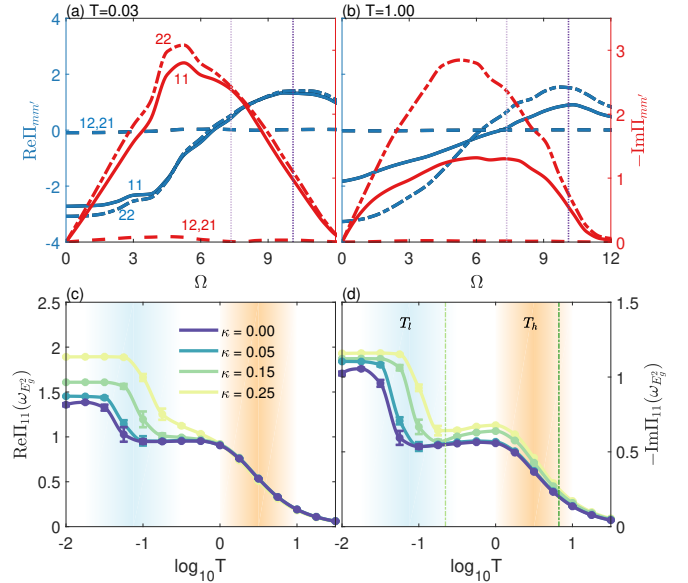


FIG. 2. The real and imaginary part of the polarization bubble $\Pi_{mm'}$ (mm' has been indicated in (a)) within a E_g channel, measured in the unit of λ_{Γ}^2 , computed by the strMC method. Panels (a-b): the frequency dependence of Re $\Pi_{mm'}$ and $-\text{Im } \Pi_{mm'}$ at different temperatures and $\kappa = 0$, corresponding to average flux densities of (a) $n_{\text{av}} = 0.01$, (b) $n_{\text{av}} = 0.48$. The two vertical purple lines denote the bare phonon energies $\omega_{E_g^1} = 7.32$ and $\omega_{E_g^2} = 10.1$. Panels (c-d): the temperature dependence of Re Π_{11} and $-\text{Im } \Pi_{11}$ evaluated at $\omega_{E_g^2}$. T_l and T_h are the two crossover temperatures. The two green vertical dashed lines in (d) indicate $T = 5K, 150K$.

expressed as $u_{\Gamma m} = \sum_{i=1}^8 u_{\Gamma m, i} q_i$, where $\Gamma = E_g^1, E_g^2$ denotes the irreps, and $m = 1, 2$ denotes the degenerate modes (see Fig.1 (b) for visualization). The corresponding free phonon Matsubara propagators can be written as $\mathcal{D}_{\Gamma m, \Gamma' m'}^{(0)}(i\omega_n) = -\langle T_{\tau} u_{\Gamma m}(\tau) u_{\Gamma' m'}(0) \rangle_{\omega_n} = \frac{2\omega_{\Gamma}}{(i\omega_n)^2 - \omega_{\Gamma}^2} \delta_{\Gamma\Gamma'} \delta_{mm'}$, where ω_{Γ} is the frequency of the optical phonon, and T_{τ} is the imaginary time ordering operator.

The *third* term in Eq.(1) is the spin-phonon coupling Hamiltonian. It originates from the change of the Kitaev interaction in response to the lattice vibration: $J(q_i) = J + \sum_{\Gamma m} \frac{dJ(q_i)}{du_{\Gamma m}} u_{\Gamma m} + \dots$, where $\frac{dJ(q_i)}{du_{\Gamma m}}$ is the gradient along $u_{\Gamma m}$ direction in the manifold of the displacement field. The D_{3d} invariant spin-phonon Hamiltonian is built as

$$H_{\text{s-ph}} = \sum_{\Gamma m} \lambda_{\Gamma} \Sigma_{\Gamma m} u_{\Gamma m}, \quad (2)$$

where $\Sigma_{E_g,1} = \sum_{\mathbf{r}} (\sigma_{\mathbf{r}}^x \sigma_{\mathbf{r}+\mathbf{M}_x}^x + \sigma_{\mathbf{r}}^y \sigma_{\mathbf{r}+\mathbf{M}_y}^y - 2\sigma_{\mathbf{r}}^z \sigma_{\mathbf{r}+\mathbf{M}_z}^z)$ and $\Sigma_{E_g,2} = \sum_{\mathbf{r}} (-\sqrt{3} \sigma_{\mathbf{r}}^x \sigma_{\mathbf{r}+\mathbf{M}_x}^x + \sqrt{3} \sigma_{\mathbf{r}}^y \sigma_{\mathbf{r}+\mathbf{M}_y}^y)$ are irreducible representations (irreps) of D_{3d} , and λ_{Γ} are the coupling constants.

Renormalization of phonon propagator.— As shown

by the perturbative calculation in the SM, the phonon propagator will be renormalized by the spin-phonon coupling. According to Dyson's equation, $\hat{\mathcal{D}} = \left[(\hat{\mathcal{D}}^{(0)})^{-1} - \hat{\Pi} \right]^{-1}$, where $\hat{\Pi}$ is the polarization bubble defined as $\Pi_{\Gamma m, \Gamma' m'} = -\lambda_{\Gamma} \lambda_{\Gamma'} \langle T_{\tau} \Sigma_{\Gamma m}(\tau) \Sigma_{\Gamma' m'}(0) \rangle$. Here, $\mathcal{D}_{\Gamma m, \Gamma' m'}$ and $\Pi_{\Gamma m, \Gamma' m'}$ are 4 by 4 matrices, where the 2 by 2 off-diagonal sub-matrices correspond to the mixing between E_g^1 , E_g^2 phonons. The 2 by 2 off-diagonal sub-matrices are negligible, since the corresponding phonon peaks in the Raman spectroscopy are well separated [24]. So next, we will focus only on the diagonal blocks of $\hat{\Pi}$, which is denoted as $\Pi_{mm'} \equiv \Pi_{\Gamma m, \Gamma m'}$.

In Fig. 2, we present the real and imaginary parts of $\Pi_{mm'}$ (blue and red curves, respectively) as functions of frequency and temperature, computed by stratified Monte Carlo method (strMC) [37]. Fig. 2(a-b) show that Π_{12} and Π_{21} are negligibly small for $\kappa = 0$, which indicates that the degenerate modes within a phonon peak are basically not mixed. Moreover, both $\text{Re} \Pi_{11}$ (blue solid curve) and $\text{Re} \Pi_{22}$ (blue dot-dash curve) are positive when evaluated at both $\omega_{E_g^1}$ and $\omega_{E_g^2}$ phonon energies, which indicates that the renormalized phonon energies are larger than bare phonon energies. This remains true and quantitatively not significantly modified even at high temperatures when Z_2 fluxes proliferate. On the other hand, the imaginary part $-\text{Im} \Pi_{mm'}$ engenders the finite phonon life-time, which gives rise to an increase of the phonon's peak width, observed in the Raman spectrum.

In Fig. 2(c-d), we focus on the E_g^2 peak and show the temperature dependence of $\Pi_{11}(\omega_{E_g^2})$ at various values of κ . Both $\text{Re} \Pi_{11}(\omega_{E_g^2})$ and $\text{Im} \Pi_{11}(\omega_{E_g^2})$ display two-stage of decrease with increased temperature, which is shared by other thermodynamics quantities in the Kitaev spin liquid [37, 48, 49]. The two crossover temperatures, namely T_l (in blue shaded area) and T_h (in orange shaded area) correspond, respectively, to the flux proliferation temperature and the major fermionic excitation temperature. While T_h is almost insensitive to κ , T_l increases with κ , which results from the increase of the Z_2 flux gap energy [37, 49].

Raman response.— The Raman scattering of the spin-phonon coupled Kitaev system (1) is described by the Raman operator: $\mathcal{R} = \sum_{\mu\mu'} (\mathcal{R}_{\text{em-ph}}^{\mu\mu'} + \mathcal{R}_{\text{em-s}}^{\mu\mu'}) E_{\text{in}}^{\mu} E_{\text{out}}^{\mu'}$, where E_{in}^{μ} , $E_{\text{out}}^{\mu'}$ are the electromagnetic fields of the incoming and outgoing lights. The second rank symmetric tensors $\mathcal{R}_{\text{em-ph}}^{\mu\mu'}$, $\mathcal{R}_{\text{em-s}}^{\mu\mu'}$ microscopically describe the polarizability change of the electronic medium in response to the excitations of phonons and spins [50]. Under the D_{3d} symmetry constraint on the Raman operator, $\mathcal{R}_{\text{em-ph}}^{\mu\mu'}$ is given by

$$\mathcal{R}_{\text{em-ph}}^{\mu\mu'} = \sum_{\Gamma m} \mu_{\Gamma} R_{\Gamma m}^{\mu\mu'} u_{\Gamma m}, \quad (3)$$

where $R_{\Gamma m}$ are the Raman tensors taken from the irreps of D_{3d} specified as

$$R_{E_g,1} = \begin{bmatrix} c & 0 & d \\ 0 & -c & 0 \\ d & 0 & 0 \end{bmatrix}, R_{E_g,2} = \begin{bmatrix} 0 & -c & 0 \\ -c & 0 & d \\ 0 & d & 0 \end{bmatrix}, \quad (4)$$

and μ_{Γ} are the coupling constants. The coupling of light to spins microscopically originates from its coupling to electric dipoles, which appears as a Wilson line operator that mediates the electronic hopping between the neighbouring ions [7, 8]. Then applying Loudon-Fleury (LF) approximation [2, 3], which is parallel to the derivation of the super-exchange interaction, the Raman operator can be obtained [51]:

$$\mathcal{R}_{\text{em-s}}^{\mu\mu'} = \nu \sum_{\alpha, \mathbf{r} \in A} \mathbf{M}_{\alpha}^{\mu} \mathbf{M}_{\alpha}^{\mu'} \sigma_{\mathbf{r}}^{\alpha} \sigma_{\mathbf{r} + \mathbf{M}_{\alpha}}^{\alpha}, \quad (5)$$

where ν is the coupling constant. $\mathcal{R}_{\text{em-s}}^{\mu\mu'}$ satisfies the symmetry constraint, which can be seen by decomposing it into the irreps of D_{3d} as $\mathcal{R}_{\text{em-s}}^{\mu\mu'} = \nu \sum_m \tilde{R}_{E_g, m}^{\mu\mu'} \Sigma_{E_g, m}$, where $\tilde{R}_{E_g, m}^{\mu\mu'} = R_{E_g, m}^{\mu\mu'} (c = 1, d = 0)$.

In this *spin-phonon coupled system*, the Raman intensity is expressed in the interaction picture as $I(\Omega) = \int dt e^{i\Omega t} \langle T_{\tau} \mathcal{R}(t) \mathcal{R}(0) e^{-i \int dt' H_{\text{s-ph}}(t')} \rangle$, where $\langle \dots \rangle = \text{Tr}[e^{-\beta H_0} \dots] / \text{Tr}[e^{-\beta H_0}]$ denotes the statistical average over the Hilbert space of the spin-phonon Hamiltonian $H_0 = H_s + H_{\text{ph}}$, $\beta = 1/T$ is the inverse temperature, and Ω refers to the inelastic energy transfer by the photon. Treating $H_{\text{s-ph}}$ as perturbation, we perform systematic evaluation of the S-matrix expansion (see SM) and obtain the Matsubara Raman correlated function:

$$\mathcal{I}(\tau) = \mathcal{I}_{\text{em-s}}(\tau) + R'_L(\tau) \cdot \hat{\mathcal{D}}(\tau) \cdot R'_R(\tau). \quad (6)$$

Here, the dot product is on the contraction of (Γ, m) indices, $R'_{\Gamma m, L(R)}(\tau) = \mu_{\Gamma} (R_{\Gamma m}^{\mu\mu'} + \mathcal{P}_{\Gamma m, L(R)}^{\mu\mu'}(\tau))$ are the renormalized left and right phonon Raman vertices, which consist of the *bare* phonon Raman vertex $\mu_{\Gamma} R_{\Gamma m}^{\mu\mu'}$ and the *spin-dependent* phonon Raman vertex $\mu_{\Gamma} \mathcal{P}_{\Gamma m, L(R)}^{\mu\mu'}(\tau)$ [42, 43] (see SM for their explicit derivation). The bare phonon Raman vertex generates the phonon peak and constitutes the dominant contribution, while the spin-dependent phonon Raman vertex generates the salient Fano line-shape. $\mathcal{I}_{\text{em-s}}^{\mu\mu'}(\tau) = -\langle T_{\tau} \mathcal{R}_{\text{em-s}}^{\mu\mu'}(\tau) \mathcal{R}_{\text{em-s}}^{\mu\mu'}(0) \rangle$ contributes to the magnetic continuum in the Raman spectrum. The physical Raman intensity is then obtained by the analytic continuation in the frequency domain: $i\Omega_n \rightarrow \Omega + i\delta_{\text{ph}}$ followed by the application of the fluctuation-dissipation theorem.

Numerical results.— With the developed formalism at hand, we now study the temperature evolution of the Raman spectrum and its κ dependence with the focus on the

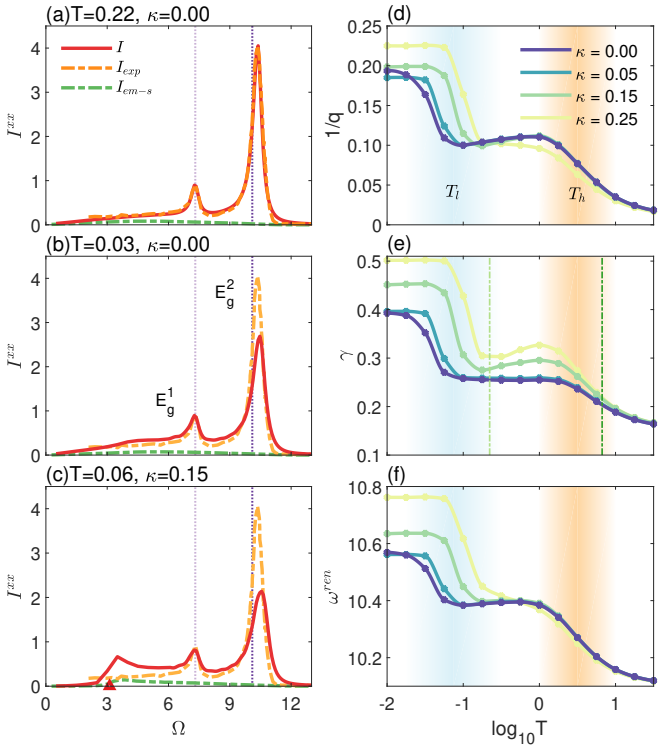


FIG. 3. Panels (a-c): The frequency dependence of MC simulated Raman intensity I at different temperatures and κ according to Eq. (6), corresponding to various average flux densities (a) $n_{av} = 0.40$, (b-c) $n_{av} = 0.01$. I_{exp} is the experimental Raman spectrum of xx geometry scattering obtained from Ref. [23] at $T = 0.22$ and $\kappa = 0$. By fitting I to the experimental intensity I_{exp} as shown in (a), the best-fit parameters of the theory can be obtained: $\omega_\Gamma = (7.31, 10.10)$, $\lambda_\Gamma = (0.20, 0.52)$, $\mu_\Gamma = (0.39, 1.10)$, $\nu = -0.60$, $\delta_{ph} = 0.15$. I_{em-s} is the pure magnetic Raman response also obtained from MC simulation. The triangle mark in (c) is twice the fermionic energy gap $2\Delta_\kappa = 12\sqrt{3}\kappa$. Panels (d-e): The temperature dependence of the E_g^2 peak curve parameters obtained from the Lorentzian fitting: $1/q$, γ and ω^{ren} . T_l and T_h are two crossover temperatures. The two green vertical dashed lines in (e) indicate $T = 5$ K and 150 K.

Fano lineshape. In the following numerical calculations, the thermodynamic average of the Raman correlation function over different flux configurations is computed by the strMC method [37] on a lattice size of $N_1 = N_2 = 20$. We will focus on xx scattering geometry in order to compare with the experiment.

To begin with, we first fix the value of the model parameters $\{\omega_\Gamma, \lambda_\Gamma, \mu_\Gamma, \nu, \delta_{ph}\}$. This is achieved by fitting the simulated Raman spectrum $I(\Omega)$ (red solid line) to the experimental Raman spectrum $I_{exp}(\Omega)$ (orange dashed line) as shown in Fig. 3(a), and the best-fit values are displayed in the caption. Here, $I(\Omega)$ is obtained via Eq. (6) and evaluated at $T = 0.22$ and $\kappa = 0$, $I_{exp}(\Omega)$ is obtained from Ref. [23] (used with permission) at the same temperature and κ , and $I_{em-s}(\Omega)$ (green dashed line) is the pure magnetic Raman response. With these

best-fit parameters, our model is able to well capture the experimental Raman spectrum. Remarkably, the best-fit parameter $\lambda_{E_g^2} = 0.52$ yields an estimation of spin-phonon coupling to be $0.52 \times \sqrt{6} = 1.3J$, (where $\sqrt{6}$ is the norm of the bilinear $\Sigma_{\Gamma m}$ in Eq. (2)), which is comparable to the first principle calculation of magnetoelastic coupling $\approx 4J$ given in Ref. [52].

Next, with fixed model parameters, we plot the simulated Raman spectrum $I(\Omega)$ for three generic values of T and κ as shown in Fig. 3(a-c). They correspond to various average Z_2 flux densities: (a) $n_{av} = 0.40$ which describes proliferated flux sectors, (b-c) $n_{av} = 0.01$ which approximates the zero-flux sector. These results display characteristic evolution of Raman spectrum in response to temperature and κ . To quantitatively characterize the spectrum, we focus on the E_g^2 peak and fit it to a Lorentzian function: $I(\Omega) = I_0 [q\gamma + (\Omega - \omega^{ren})]^2 / [\gamma^2 + (\Omega - \omega^{ren})^2]$, where $1/q$ is the asymmetry factor, γ is the half peak width, $\omega_{E_g^2}^{ren}$ is the renormalized peak position and I_0 is the peak intensity.

The temperature evolution and κ dependence of $\{1/q, \gamma, \omega^{ren}\}$ are shown in Fig. 3(d-e). First, these parameters all display two-stage change with temperature, which follows the two-stage decrease of $\text{Im} \Pi_{mm}$ and $\text{Re} \Pi_{mm}$ as analyzed above. Especially, in the T_l region, the curve parameters $\{1/q, \gamma, \omega^{ren}\}$ decreases significantly with increased flux density, which shows that they are sensitive to the emergent disorder from the proliferated Z_2 fluxes. Second, in Fig. 3(e), the decrease of half peak width γ with temperature between 5K and 150K is estimated to be $0.055J$ (see SM). This is comparable to the experimental findings in Ref. [23], that the anomalous half peak width (the deviation from the anharmonic behaviour) displays a decrease of $0.085J$ between 5K and 150K. This result indicates that the source of the anomaly comes from the spin-phonon coupling in the vicinity of the Kitaev spin liquid.

Fig. 3(d-e) show the effect of the time reversal symmetry breaking. For a fixed temperature in the region $T \lesssim T_l$, the curve parameters $\{1/q, \gamma, \omega^{ren}\}$ become larger with increased κ . This is because the finite κ lifts the fermionic spectrum with a gap $\Delta_\kappa = 6\sqrt{3}\kappa$ [29]. As κ increases, more Majorana fermions become energetically comparable to the E_g^2 phonon and participate in the spin-phonon scattering. Therefore, the curve parameters, which delineate the resultant effect of the spin-phonon scattering, become larger. Remarkably, the increase of $1/q$ and the blue shift of the phonon peak position ω^{ren} with increasing magnetic field have been observed in Ref. [26] and agree with our analysis, which can thus serve as a signature of Majorana fermions. In addition, the crossover temperature T_l is larger for larger κ , because Z_2 flux gap energy increases with κ .

Conclusion. – We have constructed a theory with D_{3d} symmetry to describe the Raman scattering of the spin-

phonon coupled Kitaev system. Based on this theory, we systematically compute the Raman spectrum and explore the temperature evolution and the magnetic field dependence of the Fano lineshape, characterized by Lorentzian curve parameters. Our results explain the phonon Raman scattering experiment in α -RuCl₃. We also identify the effect of the Majorana fermions and the emergent disorder effect from Z_2 fluxes encoded in the Fano lineshape, which provides characteristic footprints of the fractionalized excitations for experimental detection of QSL.

Acknowledgments: The authors are thankful to Ken Burch, Jia-Wei Mei, Joji Nasu, Kenya Ohgushi, Thuc T Mai, Luke Sandilands, Yiping Wang, Yang Yang, Mengxing Ye, and Shuo Zhang for valuable discussions. The work was supported by the U.S. Department of Energy, Office of Basic Energy Sciences under Award No. DE-SC0018056. N.B.P. acknowledges the hospitality of Aspen Center of Physics.

[1] T. P. Devereaux and R. Hackl, *Rev. Mod. Phys.* **79**, 175 (2007).

[2] P. Fleury and R. Loudon, *Physical Review* **166**, 514 (1968).

[3] B. S. Shastry and B. I. Shraiman, *Physical review letters* **65**, 1068 (1990).

[4] A. V. Chubukov and D. M. Frenkel, *Phys. Rev. Lett.* **74**, 3057 (1995).

[5] N. Perkins and W. Brenig, *Phys. Rev. B* **77**, 174412 (2008).

[6] N. B. Perkins, G.-W. Chern, and W. Brenig, *Phys. Rev. B* **87**, 174423 (2013).

[7] Y. Yang, M. Li, I. Rousochatzakis, and N. B. Perkins, arXiv preprint arXiv:2106.02645 (2021).

[8] W.-H. Ko, Z.-X. Liu, T.-K. Ng, and P. A. Lee, *Phys. Rev. B* **81**, 024414 (2010).

[9] J. Knolle, G.-W. Chern, D. Kovrizhin, R. Moessner, and N. Perkins, *Physical review letters* **113**, 187201 (2014).

[10] B. Perreault, J. Knolle, N. B. Perkins, and F. Burnell, *Physical Review B* **92**, 094439 (2015).

[11] B. Perreault, J. Knolle, N. B. Perkins, and F. J. Burnell, *Phys. Rev. B* **94**, 060408 (2016).

[12] B. Perreault, J. Knolle, N. B. Perkins, and F. J. Burnell, *Phys. Rev. B* **94**, 104427 (2016).

[13] J. Nasu, J. Knolle, D. L. Kovrizhin, Y. Motome, and R. Moessner, *Nature Physics* **12**, 912 (2016).

[14] I. Rousochatzakis, S. Kourtis, J. Knolle, R. Moessner, and N. B. Perkins, *Phys. Rev. B* **100**, 045117 (2019).

[15] J. Fu, J. G. Rau, M. J. P. Gingras, and N. B. Perkins, *Phys. Rev. B* **96**, 035136 (2017).

[16] A. Metavitsiadis, W. Natori, J. Knolle, and W. Brenig, arXiv preprint arXiv:2103.09828 (2021).

[17] K. W. Plumb, J. P. Clancy, L. J. Sandilands, V. V. Shankar, Y. F. Hu, K. S. Burch, H.-Y. Kee, and Y.-J. Kim, *Phys. Rev. B* **90**, 041112 (2014).

[18] J. A. Sears, M. Songvilay, K. W. Plumb, J. P. Clancy, Y. Qiu, Y. Zhao, D. Parshall, and Y.-J. Kim, *Phys. Rev. B* **91**, 144420 (2015).

[19] A. Banerjee, C. A. Bridges, J.-Q. Yan, A. A. Aczel, L. Li, M. B. Stone, G. E. Granroth, M. D. Lumsden, Y. Yiu, J. Knolle, S. Bhattacharjee, D. L. Kovrizhin, R. Moessner, D. A. Tennant, M. D. G., and S. E. Nagler, *Nat. Mater.* **15**, 733 (2016).

[20] A. Banerjee, J. Yan, J. Knolle, C. A. Bridges, M. B. Stone, M. D. Lumsden, D. G. Mandrus, D. A. Tennant, R. Moessner, and S. E. Nagler, *Science* **356**, 1055 (2017).

[21] A. Banerjee, P. Lampen-Kelley, J. Knolle, C. Balz, A. A. Aczel, B. Winn, Y. Liu, D. Pajerowski, J. Yan, C. A. Bridges, *et al.*, *npj Quantum Materials* **3**, 8 (2018).

[22] A. Little, L. Wu, P. Lampen-Kelley, A. Banerjee, S. Patankar, D. Rees, C. A. Bridges, J.-Q. Yan, D. Mandrus, S. E. Nagler, and J. Orenstein, *Phys. Rev. Lett.* **119**, 227201 (2017).

[23] L. J. Sandilands, Y. Tian, K. W. Plumb, Y.-J. Kim, and K. S. Burch, *Physical review letters* **114**, 147201 (2015).

[24] G. Li, X. Chen, Y. Gan, F. Li, M. Yan, F. Ye, S. Pei, Y. Zhang, L. Wang, H. Su, *et al.*, *Physical Review Materials* **3**, 023601 (2019).

[25] D. Wulferding, Y. Choi, S.-H. Do, C. H. Lee, P. Lemmens, C. Faugeras, Y. Gallais, and K.-Y. Choi, *Nature communications* **11**, 1 (2020).

[26] A. Sahasrabudhe, D. A. S. Kaib, S. Reschke, R. German, T. C. Koethe, J. Buhot, D. Kamenskyi, C. Hickey, P. Becker, V. Tsurkan, A. Loidl, S. H. Do, K. Y. Choi, M. Grüninger, S. M. Winter, Z. Wang, R. Valentí, and P. H. M. van Loosdrecht, *Phys. Rev. B* **101**, 140410 (2020).

[27] D. Lin, K. Ran, H. Zheng, J. Xu, L. Gao, J. Wen, S.-L. Yu, J.-X. Li, and X. Xi, *Physical Review B* **101**, 045419 (2020).

[28] Y. Wang, G. B. Osterhoudt, Y. Tian, P. Lampen-Kelley, A. Banerjee, T. Goldstein, J. Yan, J. Knolle, H. Ji, R. J. Cava, *et al.*, *npj Quantum Materials* **5**, 1 (2020).

[29] A. Kitaev, *Annals of Physics* **321**, 2 (2006).

[30] J. Knolle, D. L. Kovrizhin, J. T. Chalker, and R. Moessner, *Phys. Rev. Lett.* **112**, 207203 (2014).

[31] J. Knolle, D. L. Kovrizhin, J. T. Chalker, and R. Moessner, *Phys. Rev. B* **92**, 115127 (2015).

[32] G. B. Halász, N. B. Perkins, and J. van den Brink, *Phys. Rev. Lett.* **117**, 127203 (2016).

[33] G. B. Halász, S. Kourtis, J. Knolle, and N. B. Perkins, *Phys. Rev. B* **99**, 184417 (2019).

[34] Y. Wan and N. P. Armitage, *Phys. Rev. Lett.* **122**, 257401 (2019).

[35] A. Metavitsiadis and W. Brenig, *Physical Review B* **101**, 035103 (2020).

[36] M. Ye, R. M. Fernandes, and N. B. Perkins, *Physical Review Research* **2**, 033180 (2020).

[37] K. Feng, M. Ye, and N. B. Perkins, *Phys. Rev. B* **103**, 214416 (2021).

[38] Y. Kasahara, T. Ohnishi, Y. Mizukami, O. Tanaka, S. Ma, K. Sugii, N. Kurita, H. Tanaka, J. Nasu, Y. Motome, *et al.*, *Nature* **559**, 227 (2018).

[39] M. Ye, G. B. Halász, L. Savary, and L. Balents, *Physical review letters* **121**, 147201 (2018).

[40] Y. Vinkler-Aviv and A. Rosch, *Physical Review X* **8**, 031032 (2018).

[41] U. Fano, *Physical Review* **124**, 1866 (1961).

[42] N. Suzuki and H. Kamimura, *Journal of the Physical Society of Japan* **35**, 985 (1973).

[43] T. Moriya, *Journal of the Physical Society of Japan* **23**, 490 (1967).

[44] A. Glamazda, P. Lemmens, S.-H. Do, Y. Kwon, and

K.-Y. Choi, Physical Review B **95**, 174429 (2017).

[45] Y.-Z. You, I. Kimchi, and A. Vishwanath, Physical Review B **86**, 085145 (2012).

[46] In Ref.[45], the group element C_6^1 is modified to be $C_6^1\sigma_h$, where σ_h is a mirror reflection w.r.t the honeycomb plane. After this modification, the symmetry group is actually D_{3d} point group, which is isomorphic to C_{6v} .

[47] In our simulations we assume that the magnitude of the Kitaev interaction is $J = 2\text{meV} \approx 23K$ as estimated in [23]. While we understand that the minimal model describing $\alpha\text{-RuCl}_3$ contains other terms [53], here we show that the main features of the observed phonon dynamics can be understood already within the pure Kitaev model.

[48] J. Nasu, M. Udagawa, and Y. Motome, Physical Review B **92**, 115122 (2015).

[49] K. Feng, N. B. Perkins, and F. J. Burnell, Physical Review B **102**, 224402 (2020).

[50] M. S. Dresselhaus, G. Dresselhaus, and A. Jorio, *Group theory: application to the physics of condensed matter* (Springer Science and Business Media, 2007).

[51] In a recent study [7], some of us showed that in the Kitaev candidate materials non-LF terms also appear in the magnetic Raman scattering. However, their main effects mainly appear at energies below $1J$, so they will not change much physics at the energy scale above $1J$. This is why here we constrain our consideration to the LF approximation.

[52] D. A. Kaib, S. Biswas, K. Riedl, S. M. Winter, and R. Valentí, Physical Review B **103**, L140402 (2021).

[53] S. M. Winter, A. A. Tsirlin, M. Daghofer, J. van den Brink, Y. Singh, P. Gegenwart, and R. Valentí, **29**, 493002 (2017).

[54] T. Inui, Y. Tanabe, and Y. Onodera, *Group theory and its applications in physics*, Vol. 78 (Springer Science & Business Media, 2012).

[55] G. Guizzetti, E. Reguzzoni, and I. Pollini, Physics Letters A **70**, 34 (1979).

[56] D. S. Dummit and R. M. Foote, *Abstract algebra*, Vol. 3 (Wiley Hoboken, 2004).

[57] J.-P. Serre, *Linear representations of finite groups*, Vol. 42 (Springer, 1977).

[58] The explicit result is shared by the author through private communication.

[59] G. D. Mahan, *Many-particle physics* (Springer Science & Business Media, 2013).

[60] T. T. Mai, A. McCreary, P. Lampen-Kelley, N. Butch, J. R. Simpson, J.-Q. Yan, S. E. Nagler, D. Mandrus, A. H. Walker, and R. V. Aguilar, Physical Review B **100**, 134419 (2019).

Supplementary Material

A. The irreducible representations of the phonon modes

In the main text, we have introduced the phonon Hamiltonian H_{ph} . Its normal vibration modes will be solved by group theory. The point group we consider here is D_{3d} , which is the symmetry shared by both the Kitaev model [45] and a single layer of $\alpha\text{-RuCl}_3$ [24]. The invariance of the phonon Hamiltonian under the group operations requires $[H_{\text{ph}}, D_{3d}] = 0$. Then, to obtain the eigenmodes of H_{ph} , we apply the following theorem:

Theorem 1. *If a Hamiltonian H is invariant under the group G , ie, $[G, H] = 0$, then the irreducible representation of G forms the basis of the eigensubspace of H ; and the energy of the high dimensional irreducible representations are degenerate.*

The proof can be found in Ref. [54]. Applying this theorem to the current work, we can see that the symmetry group is D_{3d} , and the energy of the eigen vibration mode $u_{\Gamma m}$ belonging to the 2-dimensional irrep E_g is degenerate, ie, $H_{\text{ph}}u_{\Gamma m} = \omega_{\Gamma}u_{\Gamma m}$, where $\Gamma = E_g$.

As introduced in the main text, the general form of the phonon Hamiltonian can be written as $H_{\text{ph}} = H_{\text{ph}}(p_i(\mathbf{r}), q_i(\mathbf{r}))$, where $q_i(\mathbf{r}) = (x_1, y_1, z_1, \dots, x_8, y_8, z_8)_{\mathbf{r}}$ describes the displacement fields in a unit cell located at \mathbf{r} , which contains two Ru^{3+} and six Cl^- ions. $p_i(\mathbf{r})$ is the corresponding momentum. The vibration modes at the center of the Brillouin zone is classified according to the irreducible representations (irreps) of D_{3d} : $\Gamma = 2A_{1g} + 2A_{2g} + 4E_g + A_{1u} + 3A_{2u} + 4E_u$, among which the Raman active modes are $\Gamma_R = 2A_{1g} + 4E_g$ [24, 55].

Assuming that the phonon potential energy can be written as $V(q_i) = V_0 + \frac{1}{2} \sum_{i,j=1}^{24} \frac{\partial^2 V}{\partial q_i \partial q_j} \Big|_0 q_i q_j + \dots$, a vibration mode can be written as a linear combination of the displacement fields: $u_{\Gamma m}(\mathbf{r}) = \sum_i u_{\Gamma m, i} q_i(\mathbf{r})$, where Γ denotes the irreps of dimension m . As mentioned in the main text, we will drop the \mathbf{r} dependence due to long wave approximation. Then, applying linear representation theory of finite groups [54, 56, 57], we obtain the explicit form of the Raman active modes:

$$E_g^1 : \begin{cases} +0.07x_3 - 0.47z_3 - 0.07x_4 + 0.47z_4 - 0.27x_5 - 0.11y_5 - 0.23z_5 + 0.27x_6 \\ +0.11y_6 + 0.23z_6 + 0.27x_7 - 0.11y_7 + 0.23z_7 - 0.27x_8 + 0.11y_8 - 0.23z_8, \\ +0.33y_3 - 0.33y_4 - 0.11x_5 - 0.14y_5 + 0.40z_5 + 0.11x_6 \\ +0.14y_6 - 0.40z_6 - 0.11x_7 + 0.14y_7 + 0.40z_7 + 0.11x_8 - 0.14y_8 - 0.40z_8 \end{cases} \quad (7)$$

$$E_g^2 : \begin{cases} \frac{1}{\sqrt{2}}(y_1 - y_2) \\ \frac{1}{\sqrt{2}}(-x_1 + x_2) \end{cases} \quad (8)$$

$$E_g^3 : \begin{cases} -0.57x_3 - 0.06z_3 + 0.57x_4 + 0.06z_4 + 0.11x_5 - 0.27y_5 - 0.03z_5 - 0.11x_6 \\ +0.27y_6 + 0.03z_6 - 0.11x_7 - 0.27y_7 + 0.03z_7 + 0.11x_8 + 0.27y_8 - 0.03z_8, \\ +0.04y_3 - 0.04y_4 - 0.27x_5 + 0.42y_5 + 0.05z_5 + 0.27x_6 \\ -0.42y_6 - 0.05z_6 - 0.27x_7 - 0.42y_7 + 0.05z_7 + 0.27x_8 + 0.42y_8 - 0.05z_8 \end{cases} \quad (9)$$

$$E_g^4 : \begin{cases} -0.34z_3 + 0.34z_4 + 0.35x_5 + 0.20y_5 - 0.17z_5 - 0.35x_6 \\ -0.20y_6 + 0.17z_6 - 0.35x_7 + 0.20y_7 + 0.17z_7 + 0.35x_8 - 0.20y_8 - 0.17z_8, \\ -0.47y_3 + 0.47y_4 + 0.20x_5 + 0.12y_5 + 0.29z_5 - 0.20x_6 \\ -0.12y_6 - 0.29z_6 + 0.20x_7 - 0.12y_7 + 0.29z_7 - 0.20x_8 + 0.12y_8 - 0.29z_8 \end{cases} \quad (10)$$

$$A_{1g}^1 : -\frac{1}{\sqrt{2}}z_1 + \frac{1}{\sqrt{2}}z_2 \quad (11)$$

$$A_{1g}^2 : -\frac{1}{\sqrt{6}}x_3 + \frac{1}{\sqrt{6}}x_4 - \frac{1}{2\sqrt{6}}x_5 + \frac{1}{2\sqrt{2}}y_5 + \frac{1}{2\sqrt{6}}x_6 - \frac{1}{2\sqrt{2}}y_6 + \frac{1}{2\sqrt{6}}x_7 + \frac{1}{2\sqrt{2}}y_7 \\ -\frac{1}{2\sqrt{6}}x_8 - \frac{1}{2\sqrt{2}}y_8, \quad (12)$$

where the atom labeling convention followed is shown in Fig. 4.

Note that, if we consider the phonon sector alone, then each irrep has freedom of rotation by $O(2)$ matrices without changing the block-diagonal structure of the representation matrix. However, when we consider the irreps of all three sectors together, namely, the phonons, the spin bilinear products and the Raman polarization tensors, the basis needs to be fixed, such that the group operation matrices represented on this basis are the same for all three sectors. Thus, the coupling Hamiltonians built by the inner product of two sectors are invariant under group operation. In this sense, the form of the irreps (7-12) is fixed, unless the basis of all three sectors are rotated by $O(2)$ simultaneously.

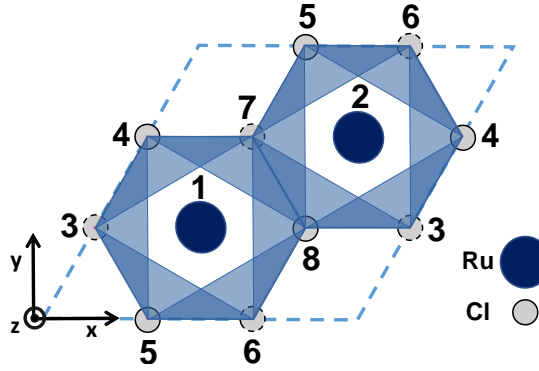


FIG. 4. Unit cell of α -RuCl₃ with labeled ions.

The modes above have been checked against the explicit results by the density functional theory (DFT) calculations [24] [58]. By comparing the energy degeneracy, energy ordering and features of the vibration modes, we identified that the low-energy modes E_g^1 and E_g^2 modes considered in [24] correspond to Eq. (7) and Eq. (8), respectively. Among the four E_g modes, E_g^2 mode Eq. (8) only involves vibration of Ru³⁺ ions. Note that, if only the vibration of Ru³⁺ ions are considered [16], the phonon modes under D_{3d} constraint decompose as $\Gamma_{Ru} = A_{1g} + E_g + A_{2u} + E_u$, where $A_{2u} + E_u$ are the three acoustic modes, and E_g and A_{1g} modes here are the same as Eq. (8) and Eq. (11). Contrary to intuition, the DFT calculations [24] suggest that this mode has higher energy than E_g^1 mode Eq. (7), in which vibrations are predominantly from Cl⁻¹ ions.

Finally, in the main text we discussed that the phonon Raman operator can be written as $\mathcal{R}_{\text{em-ph}} = \sum_{\mu, \mu'} \mathcal{R}_{\text{em-ph}}^{\mu\mu'} E_{\text{in}}^{\mu} E_{\text{out}}^{\mu'}$, where E_{in}^{μ} and $E_{\text{out}}^{\mu'}$ are the components of the electric field of incident and scattered light and the Raman vertex is given by $\mathcal{R}_{\text{em-ph}}^{\mu\mu'} = \sum_{\Gamma m} \mu_{\Gamma} R_{\Gamma m}^{\mu\mu'} u_{\Gamma m}$, where the Raman tensor for $\Gamma = E_g$ irreducible representation is defined as

$$R_{E_g,1} = \begin{bmatrix} c & 0 & d \\ 0 & -c & 0 \\ d & 0 & 0 \end{bmatrix}, R_{E_g,2} = \begin{bmatrix} 0 & -c & 0 \\ -c & 0 & d \\ 0 & d & 0 \end{bmatrix}. \quad (13)$$

We use $c = d = 1$ in numerical computations.

B. The symmetry decomposition of the Loudon-Fleury Raman operator

In the main text we introduced the explicit symmetric form of the Loudon-Fleury Raman operator

$$\mathcal{R}_{\text{em-s}} = \sum_{\mu, \mu'} \mathcal{R}_{\text{em-s}}^{\mu\mu'} E_{\text{in}}^{\mu} E_{\text{out}}^{\mu'}, \quad (14)$$

It can be expressed in terms of the irreps of D_{3d} group. Introducing a short notation $\xi^{\mu\mu'} = 1/2(E_{\text{in}}^{\mu} E_{\text{out}}^{\mu'} + E_{\text{in}}^{\mu'} E_{\text{out}}^{\mu})$, we rewrite $\mathcal{R}_{\text{em-s}} = \sum_{\mu, \mu'} \mathcal{R}_{\text{em-s}}^{\mu\mu'} \xi^{\mu\mu'}$. Then the symmetry decomposition of $\mathcal{R}_{\text{em-s}}$ according to D_{3d} can be written as $\mathcal{R}_{\text{em-s}} = \sum_{\Gamma, m} \mathcal{R}_{\text{em-s}, \Gamma m}$, where

$$\mathcal{R}_{\text{em-s}, A_g} = 1/2(\xi^{xx} + \xi^{yy})(\mathcal{R}_{\text{em-s}}^{xx} + \mathcal{R}_{\text{em-s}}^{yy}) \quad (15)$$

$$\mathcal{R}_{\text{em-s}, E_g^1} = 1/2(\xi^{xx} - \xi^{yy})(\mathcal{R}_{\text{em-s}}^{xx} - \mathcal{R}_{\text{em-s}}^{yy}) \quad (16)$$

$$\mathcal{R}_{\text{em-s}, E_g^2} = (\xi^{xy} + \xi^{yx})(\mathcal{R}_{\text{em-s}}^{xy} + \mathcal{R}_{\text{em-s}}^{yx}) \quad (17)$$

Since $[\mathcal{R}_{\text{em-s}, A_g}, H_s] = 0$, and thus only $\Gamma = E_g^1$ and $\Gamma = E_g^2$ channels contribute into the Raman response with the Raman operator given by $\mathcal{R}_{\text{em-s}} = \nu \sum_m \sum_{E_g, m} \tilde{R}_{E_g, m}^{\mu\mu'} \xi^{\mu\mu'}$. The Raman tensor $\tilde{R}_{E_g, m}^{\mu\mu'}$ is equal to the Raman tensor

$R_{E_g,m}^{\mu\mu'}$ in (13) with $c = 1, d = 0$, i.e.

$$\tilde{R}_{E_g,1} = \begin{bmatrix} 1 & 0 & 0 \\ 0 & -1 & 0 \\ 0 & 0 & 0 \end{bmatrix}, \tilde{R}_{E_g,2} = \begin{bmatrix} 0 & -1 & 0 \\ -1 & 0 & 0 \\ 0 & 0 & 0 \end{bmatrix}. \quad (18)$$

C. Perturbative calculation of the Raman response in the spin-phonon coupled Kitaev system

The spin-dependent phonon Raman scattering intensity is calculated as follows. There are two channels for the Raman scattering response, the phonon and the spin, so the Raman operator can be written as

$$\mathcal{R} = \mathcal{R}_{\text{em-ph}} + \mathcal{R}_{\text{em-s}}, \quad (19)$$

where $\mathcal{R}_{\text{em-ph}}$ and $\mathcal{R}_{\text{em-s}}$, respectively, denote the coupling of electromagnetic field of light to phonons and spins. For the simplest case, when the spins and phonons are decoupled, the general expression for the intensity is expressed as

$$I(\Omega) = \int dt e^{i\Omega t} \langle T_t \mathcal{R}(t) \mathcal{R}(0) \rangle, \quad (20)$$

where $I(t) = \langle T_t \mathcal{R}(t) \mathcal{R}(0) \rangle$ is the time-ordered Raman correlation function. It is also convenient to introduce the retarded Raman correlation function, which is also known as the Raman susceptibility:

$$\chi(\Omega) = -i \int dt e^{i\Omega t} \Theta(t) \langle [\mathcal{R}(t), \mathcal{R}(0)] \rangle. \quad (21)$$

The Raman intensity $I(\Omega)$ and the Raman susceptibility $\chi(\Omega)$ are related via the fluctuation-dissipation theorem:

$$I(\Omega) = -\frac{2}{1 - e^{-\beta\Omega}} \text{Im} \chi(\Omega). \quad (22)$$

Since we are interested in the Raman scattering at finite temperatures, we will work in the Matsubara formalism, in which the Matsubara correlation function of Raman operators is given by $\mathcal{I}(\tau) = -\langle T_\tau \mathcal{R}(\tau) \mathcal{R}(0) \rangle$ and the Fourier transform can be written as

$$\mathcal{I}(i\Omega_n) = - \int d\tau e^{i\Omega_n \tau} \langle T_\tau \mathcal{R}(\tau) \mathcal{R}(0) \rangle. \quad (23)$$

After analytical continuation $i\Omega_n \rightarrow \Omega + i\delta$, we directly obtain the retarded correlation function, i.e. the Raman susceptibility, $\chi(\Omega) = \mathcal{I}(i\Omega_n)|_{i\Omega_n \rightarrow \Omega + i\delta}$. So in the following derivation, we only need to focus on evaluating the Matsubara correlation function of the Raman operators, $\mathcal{I}(i\Omega_n)$.

Applying this mechanism, we first compute the Raman response from the decoupled phonon and spin subsystems. In this case, $\mathcal{I}^0 = \mathcal{I}_{\text{em-ph}} + \mathcal{I}_{\text{em-s}}$. The first term describes the pure phonon Raman scattering:

$$\mathcal{I}_{\text{em-ph}}^{\mu\mu'}(i\Omega_n) = \sum_{\Gamma,m} \mu_\Gamma^2 \left(R_{\Gamma m}^{\mu\mu'} \right)^2 \mathcal{D}_{\Gamma\Gamma,mm}^{(0)}(i\Omega_n) \quad (24)$$

where the scattering geometry $\mu\mu'$ has been explicitly specified, μ_Γ is the photon-phonon coupling constant in the Γ irrep and $R_{\Gamma m}^{\mu\mu'}$ is the Raman polarization tensor defined by Eq. (13) and $\mathcal{D}_{\Gamma m, \Gamma' m'}^{(0)}(i\omega_n) = \frac{2\omega_\Gamma}{(i\omega_n)^2 - \omega_\Gamma^2} \delta_{\Gamma\Gamma'} \delta_{mm'}$ is the bare phonon propagator. The corresponding Raman response is simply given by a set of delta functions at the bare phonon frequencies ω_Γ .

The second contribution comes from the magnetic Raman scattering:

$$\mathcal{I}_{\text{em-s}}^{\mu\mu'}(i\Omega_n) = - \int_0^\beta d\tau e^{i\Omega_n \tau} \langle T_\tau \mathcal{R}_{\text{em-s}}^{\mu\mu'}(\tau) \mathcal{R}_{\text{em-s}}^{\mu\mu'}(0) \rangle, \quad (25)$$

where $\mathcal{R}_{\text{em-s}}^{\mu\mu'}(\tau) = \nu \sum_m \tilde{R}_{E_g,m}^{\mu\mu'} \Sigma_{E_g,m}(\tau)$ is given in the main text and $\tilde{R}_{E_g,m}^{\mu\mu'}$ defined in Eq.(B5). The spin bilinear operator can be rewritten using the Majorana fermion representation of the spin: $\sigma_j^\alpha = i b_j^\alpha c_j$, and then transformed

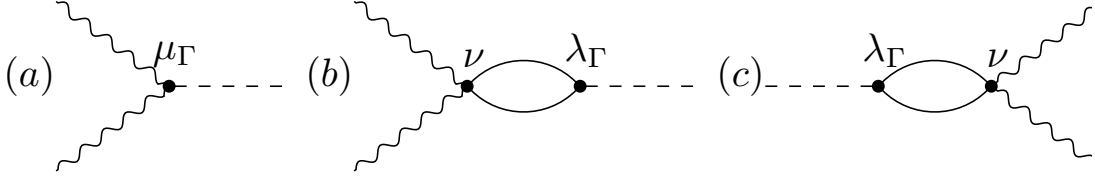


FIG. 5. The Feynman diagrams of the phonon Raman vertices: (a) $R_{\Gamma m}$ (b) $\mathcal{P}_{\Gamma m, L}$ (c) $\mathcal{P}_{\Gamma m, R}$.

into the basis of the fermionic eigenmodes. [37]. Explicitly, the correlation function of the spin Raman operators is written as a general form of $-\langle T_\tau (\mathbf{B}^\dagger \tilde{\Lambda} \mathbf{B})(\tau) (\mathbf{B}^\dagger \tilde{\Lambda} \mathbf{B})(0) \rangle$, where $\mathbf{B}^\dagger = [\beta_1^\dagger, \dots, \beta_N^\dagger, \beta_1, \dots, \beta_N]$ is the vector of the Bogoliubov quasiparticles, and $\tilde{\Lambda}$ is a symmetrized coupling matrix, whose entries are the coupling vertices between two fermion eigenmodes and the photons. Since the fermionic eigenmodes are different in different flux sectors, these coupling matrix entries are also functions of the underlying Z_2 gauge fields [37]. Finally,

$$\mathcal{I}_{\text{em-s}}^{\mu\mu'}(i\Omega_n) \sim \text{Tr} \left[\left(\mathcal{G}_1(i\omega_{n_1}) \tilde{\Lambda} \mathcal{G}_1^*(i\omega_{n_2}) \tilde{\Lambda} + \mathcal{G}_2(i\omega_{n_1}) \tilde{\Lambda} \mathcal{G}_2(i\omega_{n_2}) \tilde{\Lambda}^\top \right) \delta(i\Omega_n - i\omega_{n_1} - i\omega_{n_2}) \right], \quad (26)$$

which appears as a fermionic loop diagram. Here, $\mu\mu'$ dependence is contained inside $\tilde{\Lambda}$, and $\text{Tr}[\dots]$ sums over the Matsubara frequencies $i\omega_n$ as $T \sum_n$, and the energy conservation constraint $\Omega_n - \omega_{n_1} - \omega_{n_2} = 0$ is imposed. In the following, all fermionic loops will be evaluated in the same way. The spectrum of $\mathcal{I}_{\text{em-s}}^{\mu\mu'}$ is the magnetic continuum, which has been studied at length in the literature [9, 13, 14] and will not be repeated here.

The main goal of this work is to study the Raman response in the spin-phonon coupled Kitaev system described by the Hamiltonian (1) in the main text. The presence of spin-phonon interaction (Eq.(2) in the main text) lead to the Raman vertex renormalization due to the final-state interactions. In the interaction picture, the general expression of the Raman correlation function in the presence of the spin-phonon coupling is given by

$$I(t) = \langle T_t \mathcal{R}(t) \mathcal{R}(0) e^{-i \int dt' H_{\text{s-ph}}(t')} \rangle, \quad (27)$$

where $S = e^{-i \int dt' H_{\text{s-ph}}(t')}$ is dubbed the S -matrix. Correspondingly, at finite temperature $\mathcal{I}(\tau) = -\langle T_\tau \mathcal{R}(\tau) \mathcal{R}(0) e^{-\int_0^\beta d\tau' H_{\text{s-ph}}(\tau')} \rangle$ gives the Matsubara correlation function of the Raman operator in the spin-phonon coupled Kitaev model. Treating the coupling $H_{\text{s-ph}}$ perturbatively and using the S -matrix expansion [59], we obtain:

$$\mathcal{I}(\tau) = - \sum_{k=0}^{\infty} (-1)^k \prod_i^k \int_0^\beta d\tau_i \left\langle T_\tau \mathcal{R}(\tau) \mathcal{R}(0) \prod_i^k H_{\text{s-ph}}(\tau_i) \right\rangle \quad (28)$$

where only connected different graphs are summed. At the order of $k = 0$, this expression corresponds to the simple spin-phonon decoupled case, as described above.

At the order of $k = 1$, contribution can be explicitly written as

$$\begin{aligned} \mathcal{I}_1^{\mu\mu'}(\tau) &= \int_0^\beta d\tau_1 \left\langle T_\tau \mathcal{R}^{\mu\mu'}(\tau) \mathcal{R}^{\mu\mu'}(0) H_{\text{s-ph}}(\tau_1) \right\rangle = \begin{cases} \int_0^\beta d\tau_1 \left\langle T_\tau \mathcal{R}_{\text{em-s}}^{\mu\mu'}(\tau) \mathcal{R}_{\text{em-ph}}^{\mu\mu'}(0) H_{\text{s-ph}}(\tau_1) \right\rangle \\ \int_0^\beta d\tau_1 \left\langle T_\tau \mathcal{R}_{\text{em-ph}}^{\mu\mu'}(\tau) \mathcal{R}_{\text{em-s}}^{\mu\mu'}(0) H_{\text{s-ph}}(\tau_1) \right\rangle \end{cases} \\ &= \begin{cases} \sum_{\Gamma, m, m'} \mu_\Gamma \lambda_\Gamma R_{\Gamma m}^{\mu\mu'} \int_0^\beta d\tau_1 \left\langle T_\tau \mathcal{R}_{\text{em-s}}^{\mu\mu'}(\tau) \Sigma_{\Gamma, m'}(\tau_1) u_{\Gamma m'}(\tau_1) u_{\Gamma m}(0) \right\rangle \\ \sum_{\Gamma, m, m'} \mu_\Gamma \lambda_\Gamma R_{\Gamma m}^{\mu\mu'} \int_0^\beta d\tau_1 \left\langle T_\tau u_{\Gamma m}(\tau) \Sigma_{\Gamma, m'}(\tau_1) u_{\Gamma m'}(\tau_1) \mathcal{R}_{\text{em-s}}^{\mu\mu'}(0) \right\rangle \end{cases} \end{aligned} \quad (29)$$

which corresponds to the diagrams in Fig. 6 (c-d). At this order, it gives to the spin-dependent phonon Raman vertices (first introduced in [42, 43]), which describe the mixing term between the two channels and play the central role in generating the Fano lineshape. These two spin-dependent phonon Raman vertices, which are distinguished with notation left (L) and right (R), are given by

$$\mathcal{P}_{\Gamma m, L}^{\mu\mu'}(\tau) = -\lambda_\Gamma \left\langle T_\tau \Sigma_{\Gamma m}(\tau) \mathcal{R}_{\text{em-s}}^{\mu\mu'}(0) \right\rangle, \quad (30)$$

$$\mathcal{P}_{\Gamma m, R}^{\mu\mu'}(\tau) = -\lambda_\Gamma \left\langle T_\tau \mathcal{R}_{\text{em-s}}^{\mu\mu'}(\tau) \Sigma_{\Gamma m}(0) \right\rangle. \quad (31)$$

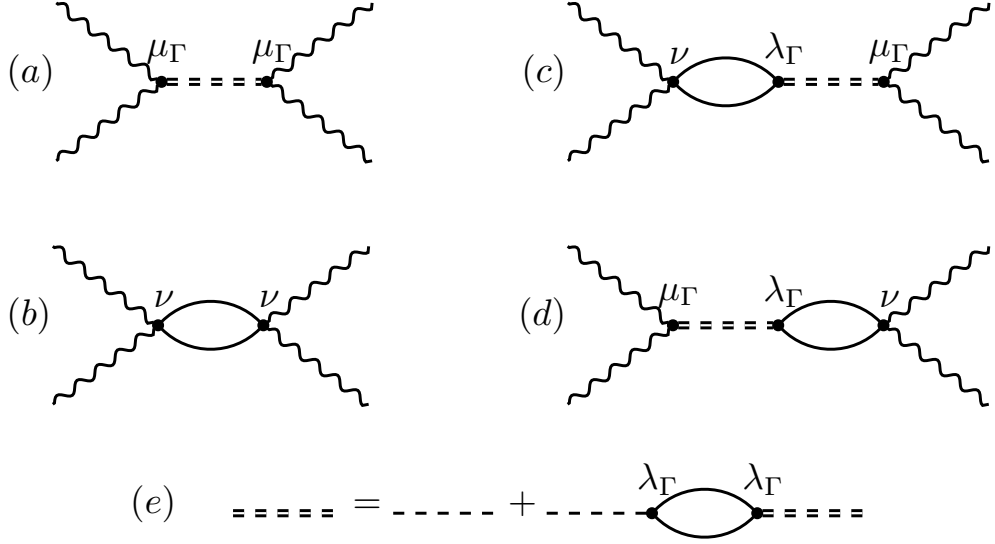


FIG. 6. The Feynman diagrams of the Raman intensity shown in Eq. (35). (a) the phonon channel with a propagator renormalized by the spin-phonon interaction (Eq.(2) in the main text), (b) the spin channel, (c)-(d) the phonon-spin mixed channel with the spin-dependent phonon Raman vertices $\mathcal{P}_{\Gamma m, L}$, $\mathcal{P}_{\Gamma m, R}$. Panel (e) shows the Dyson's equation for the phonon propagator.

The corresponding diagrams are shown in Fig. 5 (b-c). Combining $\mathcal{P}_{\Gamma m, L}^{\mu\mu'}(\tau)$ and $\mathcal{P}_{\Gamma m, R}^{\mu\mu'}(\tau)$ with the bare Raman vertex $R_{\Gamma m}^{\mu\mu'}$, we define the total left and right phonon Raman vertices as:

$$R'_{\Gamma m, L}^{\mu\mu'}(\tau) = \mu_\Gamma (R_{\Gamma m}^{\mu\mu'} + \mathcal{P}_{\Gamma m, L}^{\mu\mu'}(\tau)), \quad (32)$$

$$R'_{\Gamma m, R}^{\mu\mu'}(\tau) = \mu_\Gamma (R_{\Gamma m}^{\mu\mu'} + \mathcal{P}_{\Gamma m, R}^{\mu\mu'}(\tau)). \quad (33)$$

With these total phonon Raman vertices, the odd k terms and even k terms in the expansion Eq. (28) are grouped together, and the summation naturally forms the series that is consistent with Dyson's equation, which describes the renormalization of the phonon propagator:

$$\mathcal{D}_{\Gamma m, \Gamma' m'} = \left[[\mathcal{D}_{\Gamma m, \Gamma' m'}^{(0)}]^{-1} - \Pi_{\Gamma m, \Gamma' m'} \right]^{-1} \quad (34)$$

Here, $\Pi_{\Gamma m, \Gamma' m'}(\tau) = -\langle T_\tau \Sigma_{\Gamma m}(\tau) \Sigma_{\Gamma' m'}(0) \rangle$ is the polarization bubble. Diagrammatically, the Dyson's equation is shown in Fig. 6 (e). So, we get the phonon Raman correlation function that includes the spin-dependent phonon Raman vertices. Note that the pure spin Raman correlation function is not included in Eq.(29). Thus, the final expression of the Raman correlation function at the lowest order is given by

$$\mathcal{I}(\tau) = \mathcal{I}_{\text{em-s}}(\tau) + R'_L(\tau) \cdot \hat{\mathcal{D}}(\tau) \cdot R'_R(\tau), \quad (35)$$

where the dot product is on the contraction of (Γ, m) indices. The diagrams that give the leading order contribution to the Raman intensity in this spin-phonon coupled systems are summarized in Fig.6 (a)-(d).

D. The estimation of the width and position of the phonon peak

We now can perform an explicit calculation of the Raman phonon lineshape. Based on the Dyson equation Eq. (34), the renormalization of the phonon energy and broadening can be estimated from the polarization bubble Π . For time reversal symmetry unbroken case $\kappa = 0$, the off-diagonal components of the polarization bubble $\Pi_{mm'}$ is negligible as shown in Fig.2 in the main text. Then within a given symmetry irrep Γ , the imaginary part of diagonal

T/K	0.2	5	150	∞
γ_{est}/J	0.430	0.300	0.205	0.150
γ_{MC}/J	0.390	0.255	0.200	0.165
γ_{anom}/J		0.090	0.005	

TABLE I. The half width at half maxima (HWHM) of the E_g^2 phonon peak at several characteristic temperatures. γ_{est} is the HWHM estimated as $\gamma_{\text{est}} = \left(-\lambda_{E_g^2}^2 \text{Im} \Pi_{11} + \delta_{\text{ph}}\right)$, where $\delta_{\text{ph}} = 0.15$ and $\lambda_{E_g^2} = 0.52$ (in units of J). γ_{MC} is HWHM of E_g^2 phonon obtained from Eq. (35), evaluated with the strMC simulations on a lattice of $N_1 = N_2 = 20$ as introduced in the main text. γ_{anom} is the experimentally measured HWHM, which is the anomalous deviation from the anharmonic behaviour. It is obtained from Ref. [23], and $\gamma_{\text{anom}} = \Delta\Gamma/2$ in the notations therein. The two temperatures 5K and 150K are marked as green dot-dashed lines in Fig. 2(d) and Fig. 3(e) in the main text.

entry of the renormalized phonon propagator is given by

$$-\text{Im} D_{mm}(\Omega) = \frac{4\omega_{\Gamma}^2 \left(\frac{\Omega\delta_{\text{ph}}}{\omega_{\Gamma}} - \mu_{\Gamma}^2 \text{Im} \Pi_{mm} \right)}{(\Omega^2 - \omega_{\Gamma}^2 - 2\omega_{\Gamma}\mu_{\Gamma}^2 \text{Re} \Pi_{mm})^2 + 4\omega_{\Gamma}^2 \left(\frac{\Omega\delta_{\text{ph}}}{\omega_{\Gamma}} - \mu_{\Gamma}^2 \text{Im} \Pi_{mm} \right)^2}, \quad (36)$$

where the analytical continuation $i\Omega_n \rightarrow \Omega + i\delta_{\text{ph}}$ has been taken to obtain retarded correlation function $D_{mm}(\Omega)$, and δ_{ph} is an artificial broadening of the bare phonon peak. Then the half width at half maxima (HWHM) of the phonon peak can be estimated as

$$\gamma_{\text{est}} = \delta_{\text{ph}} - \lambda_{E_g^2}^2 \text{Im} \Pi_{mm} \quad (37)$$

Note that since we are interested in the experimentally relevant xx -scattering geometry and because of the form of the phonon Raman tensor of the E_g irrep and the explicit form of Raman tensor $R_{E_g, m}^{\mu\mu'}$ in Eq. (13), the renormalization of the position and HWHM of the E_g^2 peak are mainly controlled by Π_{11} . Since $\text{Im} \Pi_{11}$ decreases with temperature, the phonon peak width γ decreases as the temperature increases. This is shown in Tab. I, where we show $\gamma_{\text{est}} = \left(-\lambda_{E_g^2}^2 \text{Im} \Pi_{11} + \delta_{\text{ph}}\right)$ with the fitted parameter $\lambda_{E_g^2} = 0.52$ and $\delta_{\text{ph}} = 0.15$ (in units of J). As shown in Tab. I, the decrease of half peak width γ_{MC} with temperature between 5K and 150K is estimated to be $0.055J$. This is comparable to the experimental findings in Ref. [23], that the anomalous half peak width γ_{anom} displays a decrease of $0.085J$ between 5K and 150K. This result indicates that the source of the anomaly comes from the spin-phonon coupling in the vicinity of the Kitaev spin liquid. In the low-temperature region between 0.2K to 5K, the estimation of the peak width differs significantly from the strMC result. This is due to the effect of the spin-dependent phonon Raman coupling at low temperatures also causes smaller peak width.

The renormalized peak's position, $\omega_{\Gamma}^{\text{ren}}$, is given by

$$\omega_{\Gamma}^{\text{ren}} = \sqrt{\omega_{\Gamma}^2 + 2\omega_{\Gamma}\mu_{\Gamma}^2 \text{Re} \Pi_{mm}} \approx \omega_{\Gamma} + \mu_{\Gamma}^2 \text{Re} \Pi_{mm}. \quad (38)$$

Since $\text{Re} \Pi_{11} > 0$, the phonon peak moves towards right. This energy shift decreases with increasing temperature (see Fig. 3(f)) of the main text.

E. Absence of the Fano lineshape in the phonon Raman response with perpendicular polarization.

In this section, we apply our theory to analyze the polarization-resolved Raman experiment in $\alpha\text{-RuCl}_3$ reported in Ref. [60]. This work explores the Raman spectroscopy of the out-of-plane polarizations, and concludes that the spin-related effects, namely the magnetic continuum and Fano lineshape asymmetry, disappear when the photon polarization is perpendicular to the honeycomb plane of Ru ions, suggesting that these effects are both of the same two-dimensional origin.

To explore the polarization dependence of the Raman spectroscopy, Eq. (35) needs to be explicitly evaluated. Following the same set up in Ref. [24], for polarization within the a - c plane, we denote the angle between E and a axis as ϕ . Consider parallel scattering geometry, $E_{\text{in}} = E_{\text{out}} = [\cos \phi, 0, \sin \phi]$. Then the Raman intensity is proportional

to

$$\cos^4 \phi \mathcal{I}^{xx} + \sin^4 \phi \mathcal{I}^{zz} + \cos^2 \phi \sin^2 \phi \mathcal{I}^{xz} + \sin^2 \phi \cos^2 \phi \mathcal{I}^{zx}, \quad (39)$$

where $\mathcal{I}^{\mu\mu'}$ is defined in Eq. (35). We focus on the perpendicular polarization $\phi = \pi/2$ so only \mathcal{I}^{zz} is considered. First we analyze the phonon peak in the Raman spectrum, which is contributed from the phonon Raman tensor $R_{\Gamma,m}^{\mu\mu'}$. As shown in Eq. (13), $R_{\Gamma,m}^{zz} = 0$ for D_{3d} group, which indicates that so the response in the zz polarization would be identically zero. But if the symmetry is broken to C_{2h} , as shown in Ref. [24], the non-zero $R_{\Gamma,m}^{zz}$ is allowed so the phonon peak persists at $\phi = 0$ there. Therefore, the nonzero peak in the Raman spectrum at perpendicular polarization observed in Ref. [60] must result from the symmetry breaking from D_{3d} to C_{2h} . This symmetry breaking is introduced from the distortion of the honeycomb lattice due to the weak interlayer interaction [60].